J Neurophysiol 120: 171–185, 2018.
First published March 28, 2018; doi:10.1152/jn.00389.2017.

RESEARCH ARTICLE | *Sensory Processing*

Differential effects of adaptation on odor discrimination

Seth Haney,[1] Debajit Saha,[2] Baranidharan Raman,[2] and Maxim Bazhenov[1]
[1]*Department of Medicine, University of California, San Diego, La Jolla, California; and* [2]*Department of Biomedical Engineering, Washington University in St. Louis, St. Louis, Missouri*

Submitted 26 May 2017; accepted in final form 23 March 2018

Haney S, Saha D, Raman B, Bazhenov M. Differential effects of adaptation on odor discrimination. *J Neurophysiol* 120: 171–185, 2018. First published March 28, 2018; doi:10.1152/jn.00389.2017.— Adaptation of neural responses is ubiquitous in sensory systems and can potentially facilitate many important computational functions. Here we examined this issue with a well-constrained computational model of the early olfactory circuits. In the insect olfactory system, the responses of olfactory receptor neurons (ORNs) on the antennae adapt over time. We found that strong adaptation of sensory input is important for rapidly detecting a fresher stimulus encountered in the presence of other background cues and for faithfully representing its identity. However, when the overlapping odorants were chemically similar, we found that adaptation could alter the representation of these odorants to emphasize only distinguishing features. This work demonstrates novel roles for peripheral neurons during olfactory processing in complex environments.

NEW & NOTEWORTHY Olfactory systems face the problem of distinguishing salient information from a complex olfactory environment. The neural representations of specific odor sources should be consistent regardless of the background. How are olfactory representations robust to varying environmental interference? We show that in locusts the extraction of salient information begins in the periphery. Olfactory receptor neurons adapt in response to odorants. Adaptation can provide a computational mechanism allowing novel odorant components to be highlighted during complex stimuli.

adaptation; olfaction; receptor neurons; temporal code

INTRODUCTION

Sensory systems are responsible for representing sensory cues encountered in the surrounding environment quickly and reliably. A fundamental computational problem to be overcome is thus extracting salient information from a noisy environment contaminated with less important background signals (Rokni et al. 2014). Furthermore, how do sensory systems maintain the representation of the stimulus regardless of other competing cues, and what mechanisms may play important roles in achieving this computation?

Adaptation has been proposed as a mechanism to distinguish between background and foreground olfactory objects in rats (Kadohisa and Wilson 2006; Linster et al. 2007). In these studies, adaptation serves as a filter to increase sensitivity to novel stimuli. However, these studies identify the locus of adaptation centrally, within the anterior piriform cortex, many synapses away from the sensory neurons. Sensory systems such as vision (Burns and Baylor 2001; Hardie and Raghu 2001) and audition (Hudspeth and Gillespie 1994; Ricci et al. 1998) begin complex computations right at the level of sensory neurons. It remains unclear what role adaptation at the peripheral sensory neuron may play in olfaction and how this might impact computational aspects of foreground-background odor separation.

In the insect olfactory system, odorants are transduced into electrical signals by olfactory receptor neurons (ORNs) in the antennae and are transmitted to downstream centers for further processing. ORNs respond to odorants with peaked transient responses and moderate responses at steady state of long pulses (Raman et al. 2010; Saha et al. 2013). The transition from peak to steady-state firing rate is called adaptation. While much of the study of odor coding has focused on the downstream antennal lobe (AL) (Bazhenov et al. 2001a; Galizia and Sachse 2010; Ito et al. 2009; Laurent et al. 1996; Riffell et al. 2009; Wehr and Laurent 1996, 1999), peripheral ORNs may play a large, and underexamined, role in temporal patterning and odor coding (Raman et al. 2010). In particular, sensory neuron adaptation and its roles in temporal coding (Raman et al. 2010; Wehr and Laurent 1996) and background separation (Kadohisa and Wilson 2006; Linster et al. 2007; Saha et al. 2013) are not well understood. The goal of this work was to investigate how adaptation of ORNs can impact reliable odor coding in a complex odor environment.

The locust olfactory pathway has been instrumental in understanding neural coding mechanisms including odor identity, intensity, dynamics, and memory (Bazhenov et al. 2001a; Laurent et al. 1996; Laurent and Davidowitz 1994; Mazor and Laurent 2005; Perez-Orive et al. 2002; Stopfer et al. 1997, 2003). Recently, we have shown that other intricate functions, such as odor recognition in complex background and novelty detection, can be achieved by the AL circuit (Saha et al. 2013, 2015). Using an appetitive and innate behavioral assay, we have also shown that the neural prediction matches well with the behavioral outcomes (Saha et al. 2013, 2015; Simões et al. 2011). However, it is still unknown what role adaptation of the ORNs plays in determining this success. Moreover, it is known that spatiotemporal patterning in the AL is critically dependent on the temporal pattering of ORN responses (Raman et al. 2010). All of these findings make ORN adaptation an important topic of investigation toward understanding the role of these peripheral neurons in recognition of a novel stimulus in a complex environment.

Address for reprint requests and other correspondence: M. Bazhenov, 9500 Gilman Dr., La Jolla, CA 92093-7381 (e-mail: mbazhenov@ucsd.edu).

Here we approach these questions using a combination of electrophysiological measurements and a biophysically realistic model of the ORNs and the AL circuitry.

METHODS

Odor Stimulation

Odorants were delivered according to a standard protocol described in an earlier work (Brown et al. 2005). Briefly, odor solutions were diluted in mineral oil to 1% concentration (vol/vol) and placed in 60-ml glass bottles. Odor pulses were delivered by injection of a constant volume (100 ml/min) of the static headspace above the odorants into a desiccated airstream (750 ml/min) flowing continuously across the antenna. A large vacuum funnel was placed behind the locust preparation to continuously remove the delivered odorants. The following odorants were used in this study: 2-octanol, hexanol, cyclohexanone, 2-heptanone, benzaldehyde, isoamyl acetate, hexanal, geraniol, citral, peppermint, and apple. Each stimulus was presented multiple times in one or two pseudorandomized blocks of five trials. The interstimulus interval was at least 60 s for all recordings.

Electrophysiology

Electrophysiological experiments were conducted in locusts (*Schistocerca americana*) raised in a crowded colony. Young adults (after the fifth instar) of either sex were used. ORN recordings were made from different sensilla types in intact but immobilized locust antennae as described previously (Raman et al. 2010). The antenna was stabilized with wax, and a reference electrode (Ag/AgCl wire) was inserted into the locust gut. Single-sensillum recordings were made with saline-filled glass micropipettes (≈10-μm diameter, 5–10 MΩ) that were inserted into the base of the sensillum. Acquired signals were amplified with a differential amplifier (Grass P55), filtered between 0.3 and 10.0 kHz, and acquired at a 15-kHz sampling rate (PCI-MIO-16E-4 DAQ cards; National Instruments). Multiunit single-sensillum recordings were spike sorted off-line with Spike-o-Matic software (Pouzat et al. 2002) implemented in IGOR Pro (WaveMetrics).

To monitor activity in the AL, locusts were immobilized with both antennae intact and the brain was exposed, desheathed, and superfused with locust saline at room temperature. In the AL, multiunit tetrode recordings were made with 16-channel, 4 × 4 silicon probes (NeuroNexus). These electrodes were electroplated with gold to obtain impedances in the 200–300 kΩ range. A custom-made 16-channel amplifier (Biology Electronics Shop, Caltech, Pasadena, CA) was used to collect projection neuron data at 15 kHz. The data were amplified at a 10,000 gain, filtered between 0.3 and 6 kHz ranges, and saved with a LabVIEW data acquisition system. To allow the assignment of recorded spikes to unique cell sources, spike sorting was done off-line with the best three or four channels recorded and conservative statistical principles (Pouzat et al. 2002). A total of 119 ORNs were recorded from 27 locusts, and 725 projection neurons (PNs) were recorded from 70 locusts.

Adaptation Calculation

The level of ORN adaptation (P_{adp}) is defined by the quantity

$$P_{adp} = 1 - \frac{\text{steady state} - \text{baseline firing}}{\text{peak firing} - \text{baseline firing}}$$

To reduce fast variation in adaptation calculations, we average over the population of ORNs and filter this mean signal with a zero-phase digital filter (MATLAB's filtfilt). The peak firing rate was calculated as the maximum firing rate over the first 2 s after stimulus. The steady-state firing rate was determined by averaging over the time window t = 2–4 s after stimulus. The baseline firing rate is calculated as the average firing rate over the first second before stimulus.

Olfactory Receptor Model

The code used to simulate this model is available on our laboratory website (https://www.bazhlab.ucsd.edu/downloads/). The olfactory receptor model is based on a stochastic state transition scheme in which each receptor can be in one of three discrete states: silent (*S*), firing (*F*), or desensitized (*D*). The transitions between states are based on a Monte Carlo method where a draw of random numbers determines *1*) when the next transition of any ORN's state will occur based on the sum of the propensities of all possible transitions and *2*) which ORN state transition will occur based on each individual propensity (Gillespie 1976, 1977; also see outline below). The transition propensities β, γ, and δ represent the $F\rightarrow S$, $F\rightarrow D$, and $D\rightarrow S$ transitions, respectively. The $S\rightarrow F$ transition is dependent on a propensity parameter, an alignment of odor with receptor x, and the concentration of the odorant at a given time, $\alpha\cdot A(x)\cdot B(x,t)$, where the odorant concentration depends on the ORN cell number, x, and on time, t. The ORN alignment, $A(x)$, is given by a Gaussian function with peak value 4. The mean of this Gaussian determines the odor identity, and the standard deviation, σ, determines the concentration—increasing concentration has been shown to increase the population of responding neurons, not the level of response (see Ito et al. 2009). Here we used σ = 900, or 10% of the total number of ORNs. The temporal dependence of this function is given by a pulse function $B(x,t) = H[t - t_{on}(x)] - H[t - t_{off}(x)]$, where $H(t)$ are step functions and $t_{on}(x)$ and $t_{off}(x)$ are the on and off times of the odorant. They both depend on the cell number because we added a cell-specific random delay for the onset and offset of the odorant modeled by a uniform random variable with max 500 ms. This delay is based on the observed variable time from stimulus onset to ORN response seen in electrophysiological recordings of ORNs (not shown).

We used the Gillespie exact stochastic simulation algorithm (ESSA) (Gillespie 1976) to simulate the ORN model. The model was divided into discrete events. The calculation of the state of the system at a future time was designed as a four-step process (Gillespie 1976, 1977):

1. Each state transition event was assigned a probability of occurring, a_i, based on the propensity parameters given in Table 1 and the current state of the ORNs. For example, $a_i = \alpha\cdot A(x_i)\cdot B(x_i,t)$ for an $S\rightarrow F$ transition and $a_i = \beta$ for an $F\rightarrow S$ transition. The index i runs over all ORNs and possible transitions. The probability that event i occurs in the next small increment of time, τ, is τa_i.
2. The time to the next event of any type was then calculated as a Poisson process. Thus interevent times are exponentially distributed with parameter $\lambda = \Sigma_i a_i$. Drawing a random number from this distribution, we obtain the time increment Δt.
3. A final random number was drawn to determine which event occurred. Here, each event occupies a proportion equal to a_i/λ of the unit interval.

Table 1. *Propensities used to simulate ORN model*

P_{adp}	α	β	γ	δ
0.1025	0.1000	0.1000	0.0090	0.0060
0.1943	0.1000	0.1000	0.0062	0.0033
0.2977	0.1000	0.1000	0.0054	0.0022
0.3915	0.1000	0.1000	0.0041	0.0015
0.4996	0.1000	0.1000	0.0034	0.0009
0.5979	0.1000	0.1000	0.0024	0.0005
0.7030	0.1000	0.1000	0.0017	0.0002

Transition propensities α, β, γ, and δ represent the $S\rightarrow F$, $F\rightarrow S$, $F\rightarrow D$, and $D\rightarrow S$ transitions respectively, where S is silent, F is firing, and D is desensitized. ORN, olfactory receptor neuron; P_{adp}, level of ORN adaptation.

4. The selected reaction was executed, the ORN states were updated, and time was incremented by Δt.

To find parameters that conferred the desired adaptation properties, we performed an exhaustive parameter search to find parameters α, β, γ, δ. Parameters were selected so that maximal firing rate did not differ more than $\pm 5\%$ between adaptation levels; only steady state was affected. In our simulations, every ORN is assigned the same parameters for a given level of adaptation. The parameters used are given in Table 1.

Receptors only passed input to the AL in the firing state. Each PN received input from 30 ORNs in regular fashion (e.g., 1st PN received input from *ORNs 1–30*, 2nd PN received input from *ORNs 31–60*, etc.; see also Fig. 2). Similarly, each local neuron (LN) received input from 90 ORNs. This input produced a current given by

$$I_{\text{stim},i} = g_{\text{stim}} \| F_i \|$$

where $\|F_i\|$ is the count of ORNs connected to PN_i that are in the firing state at a given time step (see below for current I_{stim}) and $g_{\text{stim}} = 1.43$ μS is the conductance. The ORN firing rate is calculated by counting of the number of ORNs in the firing state for each time step summed over the time bin divided by the amount of time in the bin.

Antennal Lobe Model

The code used to simulate this model has been described previously (Assisi et al. 2007, 2011; Bazhenov et al. 2001a, 2001b; Kee et al. 2015; Sanda et al. 2016) and is available on our laboratory website (https://www.bazhlab.ucsd.edu/downloads/). The locust contains ~850 PNs and ~300 LNs. We modeled a scaled-down 300 PNs and 100 LNs with single compartments that included voltage- and Ca^{2+}-dependent currents described by Hodgkin-Huxley kinetics (Hodgkin and Huxley 1952). Parameterization was done to minimize the number and complexity of ionic currents in each cell type and generate realistic (though simplified) firing profiles. No attempt was made to produce intrinsic resonant oscillations (pacemaker properties) in LNs or PNs because such properties have never been observed in locust LNs or PNs (Laurent 1996; Laurent and Davidowitz 1994). The model was constrained to produce population oscillations [local field potential (LFP)] in the AL and cellular responses as observed in vivo (Bazhenov et al. 2001a). Model equations were solved with a fourth-order Runge-Kutta method with an integration time step of 0.04 ms.

Membrane potentials. PN and LN membrane potential equations (Hodgkin and Huxley 1952) are given by

$$C_{\text{m}}\frac{\text{d}V_{\text{PN}}}{\text{d}t} = -g_{\text{L}}\left(V_{\text{PN}} - E_{\text{L}}\right) - I_{\text{Na}} - I_{\text{K}} - I_{\text{A}} - g_{\text{KL}}\left(V_{\text{PN}} - E_{\text{KL}}\right) - I_{\text{GABA}_{\text{A}}} - I_{\text{nACh}} - I_{\text{stim}}$$

$$C_{\text{m}}\frac{\text{d}V_{\text{LN}}}{\text{d}t} = -g_{\text{L}}\left(V_{\text{LN}} - E_{\text{L}}\right) - I_{\text{Ca}} - I_{\text{K(Ca)}} - I_{\text{K}} - g_{\text{KL}}\left(V_{\text{PN}} - E_{\text{KL}}\right) - I_{\text{GABA}_{\text{A}}} - I_{\text{nACh}} - I_{\text{stim}}$$

The LN passive parameters are given $C_{\text{m}} = 1$ μF (membrane capacitance), $g_{\text{L}} = 0.15$ μS (conductance for the leak current), $g_{\text{KL}} = 0.02$ μS (conductance for the potassium leak current), $E_{\text{L}} = -50$ mV (reversal potential for the leak current), and $E_{\text{KL}} = -95$ mV (reversal potential for the potassium leak current). The PN passive parameters are the same as LN except $E_{\text{L}} = -55$ mV and $g_{\text{KL}} = 0.05$ μS. An external DC input was introduced to each neuron through I_{stim}.

Intrinsic currents. The sodium current (I_{Na}) (see Traub et al. 1997) is given by

$$I_{\text{Na}} = g_{\text{Na}} m^3 h \left(V - E_{\text{Na}}\right)$$

where the conductance in PNs is $g_{\text{Na}} = 7.15$ μS and the reversal potential is $E_{\text{Na}} = 50$ mV. The gating variables satisfy the equations

$$\frac{\text{d}m}{\text{d}t} = -\frac{1}{\tau_m}\left[m - m_\infty(V)\right]$$

$$\frac{\text{d}h}{\text{d}t} = -\frac{1}{\tau_h}\left[h - h_\infty(V)\right]$$

The steady-state values of the gating variables are given by

$$m_\infty(V) = \frac{1}{1 + \exp\left(-\dfrac{V + 20}{6.5}\right)}$$

$$h_\infty(V) = \frac{1}{1 + \exp\left(-\dfrac{V + 25}{12}\right)}$$

The time constants are $\tau_m = 1.5$ and

$$\tau_h = 0.3\exp\left(\frac{V - 40}{13}\right) + 0.002\exp\left(-\frac{V - 60}{29}\right)$$

The fast potassium current (I_{K}) (see Traub et al. 1997) is given by

$$I_{\text{K}} = g_{\text{K}} n^4 \left(V - E_{\text{K}}\right)$$

where the conductance in LNs is $g_{\text{K}} = 10$ μS and the reversal potential is $E_{\text{K}} = -95$ mV. In the PNs, $g_{\text{K}} = 1.43$ μS and $E_{\text{K}} = -95$ mV. The equation for the gating variable n is given by

$$\frac{\text{d}n}{\text{d}t} = -\frac{1}{\tau_n}\left[n - n_\infty(V)\right]$$

where the steady-state value, n_∞, and the time constant, τ_n, are nonlinear functions of V and given by

$$n_\infty = \frac{\alpha_n}{\left(\alpha_n + \beta_n\right)\varphi}$$

$$\tau_n = \frac{1}{\left(\alpha_n + \beta_n\right)\varphi}$$

where

$$\alpha_n = 0.02\frac{15 - \left(V + 50\right)}{\exp\left[\dfrac{15 - \left(V + 50\right)}{5}\right] - 1}$$

and

$$\beta_n = 0.5\exp\left[\frac{10 - \left(V + 50\right)}{40}\right]$$

The variable φ depends on the temperature and is given by $\varphi = 3^{\left(\frac{22-36}{10}\right)} = 3^{-1.4}$ at 36°C.

The Ca^{2+} current (I_{Ca}) (see Laurent et al. 1993) is given by

$$I_{\text{Ca}} = g_{\text{Ca}} m^2 h \left(V - E_{\text{Ca}}\right)$$

where $g_{\text{Ca}} = 2$ μS and $E_{\text{Ca}} = 140$ mV. The gating variables satisfy the equations

$$\frac{\text{d}m}{\text{d}t} = -\frac{1}{\tau_m}\left[m - m_\infty(V)\right]$$

$$\frac{\text{d}h}{\text{d}t} = -\frac{1}{\tau_h}\left[h - h_\infty(V)\right]$$

The steady-state values of the gating variables are given by

$$m_\infty(V) = \frac{1}{1 + \exp\left(-\frac{V+20}{6.5}\right)}$$

$$h_\infty(V) = \frac{1}{1 + \exp\left(-\frac{V+25}{12}\right)}$$

The time constants are $\tau_m = 1.5$ and

$$\tau_h = 0.3\exp\left(\frac{V-40}{13}\right) + 0.002\exp\left(-\frac{V-60}{29}\right)$$

The calcium-dependent potassium current [$I_{K(Ca)}$] (see Sloper and Powell 1979) is given by

$$I_{K(Ca)} = g_{K(Ca)} m^2 h\left[V - E_{K(Ca)}\right]$$

where $g_{K(Ca)} = 0.3$ μS and $E_{K(Ca)} = -90$ mV. The gating variable satisfies the equation

$$\frac{dm}{dt} = -\frac{1}{\tau_m + \tau_x}\left[m - m_\infty(V)\right]$$

while

$$m_\infty(V) = \frac{\left[Ca^{2+}\right]}{\left[Ca^{2+}\right] + 2}$$

$$\tau_m = \frac{100}{\left[Ca^{2+}\right] + 2}$$

and τ_x is obtained from a uniform distribution extending from -0.02 to 0.01. Calcium concentration ([Ca^{2+}]) satisfies a simple first-order equation:

$$\frac{d\left[Ca^{2+}\right]}{dt} = -AI_{Ca}\frac{\left[Ca^{2+}\right] - \left[Ca^{2+}\right]_\infty}{\tau}$$

where $[Ca^{2+}]_\infty = 2.4 \times 10^{-4}$ mM is the equilibrium of intracellular [Ca^{2+}], $A = 5.2 \times 10^{-4}$ mM·cm^2/(ms·μA), and $\tau = 5$ ms.

The transient potassium A current (I_A) (see Huguenard et al. 1991) is given by

$$I_A = g_A m^4 h\left(V - E_A\right)$$

where $g_A = 10$ μS and $E_A = -95$ mV. The gating variables satisfy the equations

$$\frac{dm}{dt} = -\frac{1}{\tau_m}\left[m - m_\infty(V)\right]$$

$$\frac{dh}{dt} = -\frac{1}{\tau_h}\left[h - h_\infty(V)\right]$$

The steady-state values of the gating variables are given by

$$m_\infty(V) = \frac{1}{1 + \exp\left(-\frac{V+60}{8.5}\right)}$$

$$h_\infty(V) = \frac{1}{1 + \exp\left(-\frac{V+78}{6}\right)}$$

The time constants were given by

$$\tau_m = \frac{0.25}{\left[\exp\left(\frac{V+35.8}{19.7}\right) + \exp\left(-\frac{V+79.7}{12.7}\right) + 0.09\right]}$$

and

$$\tau_h = \frac{0.25}{\left[\exp\left(\frac{V+46}{5}\right) + \exp\left(-\frac{V+238}{37.5}\right)\right]}$$

if $V < -63$ mV and $\tau_h = 4.8$ if $V \geq -63$ mV.

Synaptic currents. Fast GABA and nicotinic cholinergic synaptic currents to LNs and PNs (Laurent 1996) are modeled by first-order activation schemes (Destexhe et al. 1994). Fast GABA and cholinergic synaptic currents are given by

$$I_{syn} = g_{syn}\left[O\right]\left(V - E_{syn}\right)$$

where the reversal potential is $E_{nACh} = 0$ mV for cholinergic receptors and $E_{GABA_A} = -70$ mV for fast GABA receptors. The fraction of open channels, [O], is calculated according to the equation

$$\frac{d\left[O\right]}{dt} = \alpha\left(1 - \left[O\right]\right)\left[T\right] - \beta\left[O\right]$$

For cholinergic synapses transmitter concentration, [T], is given by

$$\left[T\right] = AH\left(t_0 - t_{max} - t\right)H\left(t - t_0\right)$$

and for GABAergic synapses

$$\left[T\right] = \frac{1}{1 + \exp\left(-\frac{V - V_0}{\sigma}\right)}$$

where H is the Heaviside step function (Korn and Korn 1968), t_0 is the time of receptor activation, $A = 0.5$, $t_{max} = 0.3$ ms, and $\sigma = 1.5$. The rate constants were given as $\alpha = 10$ ms^{-1} and $\beta = 0.16$ ms^{-1} for GABA synapses and $\alpha = 10$ ms^{-1} and $\beta = 0.2$ ms^{-1} for cholinergic synapses. The peak synaptic conductances were set to $g_{GABA_A} = 4 \times 10^{-4}$ between LNs, $g_{GABA_A} = 2 \times 10^{-4}$ from LNs to PNs, and $g_{ACh} = 5 \times 10^{-4}$ μS from PNs to LNs.

Network geometry. In the locust AL, LNs are synaptically connected to other LNs and to PNs (Leitch and Laurent 1996). Both LNs and PNs receive direct synaptic input from ORNs (Laurent 1996). All network interconnections were random with 0.5 probability, suitable for our scaled-down network (Assisi et al. 2012; Bazhenov et al. 2001b; Kee et al. 2015). Some of the intrinsic parameters of the neurons in the network were initialized with random variability to ensure robust results.

Classification

For both model and experiment, we considered ensemble PN spike counts in a 50-ms nonoverlapping time bin as a high-dimensional response vector. Response vectors obtained during solitary foreground and background odor exposures were regarded as the desired reference templates to be pattern matched. Trial-averaged (5 trials experiment, 10 trials model) reference templates were generated for each odor (4-s pulse duration). These reference templates, representing the mean ensemble PN activity during the 4-s window after odor onset, were then compared to test trials using angular distance. Angular distance, θ, between a given test vector ($\mathbf{V_t}$) and each reference vector ($\mathbf{V_r}$) was computed as follows:

$$\theta = \cos^{-1}\left(\frac{\mathbf{V_t} \cdot \mathbf{V_r}}{\|\mathbf{V_t}\| \cdot \|\mathbf{V_r}\|}\right)$$

To identify meaningful response patterns, only test vectors that met the appropriate criteria were compared. First, we defined a threshold length that must be exceeded by a vector to be considered an odor-evoked response. The threshold was set as the mean (over trials and time bins) of the Euclidean norm (over PNs) of the prestimulus activity vectors + 2 standard deviations of this mean. Second, we defined a tolerance threshold that would restrict the classification analysis to include only those vectors that are within a certain angular distance to any one of the desired response templates. An 85° angular distance threshold was used for classification analyses. Only those test vectors that exceeded the detection threshold but were within the defined tolerance threshold were classified. Each classified test vector was assigned to the same odor category as its best-matching reference template, background or foreground. In the model, distinct trials were created by using different random seeds in the simulation of the ORN model. Our stochastic state scheme ORN model created a large amount of trial-to-trial variance.

Responsive PNs and Coactivation

For a PN to be considered as "responsive" to an odor, the following two criteria had to be satisfied: *1*) amplitude criterion: odor-evoked average (over trials) neural activity in at least one of the time bins during odor presentation window must exceed 6.5 standard deviations of average baseline activity (response in a 1-s window before odor onset) and *2*) reliability criterion: the amplitude criterion has to be met in at least 50% of total trials. In other words, the peak activity must exceed this standard in both the average over trials and 50% of trials.

Coactivated PNs were those that were responsive to both odorants, and thus the percentage of coactivated PNs, C, is given by

$$C = 100 \times \frac{\text{PNs responsive to both odors}}{\text{PNs responsive to second odor}}$$

RESULTS

Adaptation of ORNs in Vivo

Adaptation of peripheral neurons to prolonged olfactory exposure is well characterized across vertebrates and invertebrates, specifically in the locust (Brown et al. 2005; Dalton 2000; Hendin et al. 1994; Kadohisa and Wilson 2006; Raman et al. 2010; Verhagen et al. 2007). Sensory neuron adaptation is particularly important in invertebrates for establishing the temporal component to olfactory coding (Laurent et al. 1996; Raman et al. 2010). However, it is still unclear how ORN adaptation may depend on odor identity or affect downstream odor coding in a complex odor environment.

To quantify ORN adaptation, we exposed locusts to long odor pulses (4 s) and recorded from ORNs. We found, in agreement with previous results (Saha et al. 2013), that on average ORN activity in response to odor stimulus displays several distinct temporal phases. Before odor onset, ORNs fired action potentials at a baseline rate. Upon odor onset the ORNs displayed a strong transient firing phase, which then adapted to a steady-state activity within ~1.5 s from odor onset. Note that the steady-state activity was typically elevated over baseline activity. Finally, at odor offset, ORN activity returned to the baseline firing rate smoothly from the steady-state firing rate (Fig. 1*A*). However, the degree to which ORNs adapted from the peak firing rate to the steady-state levels varied dramatically. We quantified ORN adaptation properties using the P_{adp} measure that gives a percentage of adaptation from peak response rate to steady-state ORN firing rate (see METHODS). We found that the total level of adaptation, P_{adp}, over all odors tested ranged from 0.18 to 0.90 (Fig. 1, *B–D*). Chemical specificity of receptors selects a distinct subset of ORNs with definitive adaptation properties. This produces an adaptation profile that is odor dependent. These data on variability in adaptation of the ORN firing rates in vivo (Fig. 1*D*, *inset*) were used to create a biophysically accurate model in silico.

How might these large differences in adaptation affect downstream temporal coding? How does this affect the ability of the olfactory system to reliably respond to novel stimuli in a complex odor environment? To answer these questions, we built a stochastic model of olfactory receptors that incorporated receptor desensitization. This model reproduced the vast amount of diversity in adaptation mentioned above and had profound impacts on downstream coding of odors.

Stochastic Model of ORN Dynamics

We constructed a stochastic model of the individual ORNs based on the linear kinetic transitions between three states: silent, firing, and desensitized states. We provide a brief description of the model here and a detailed description in METHODS. ORNs passed input to the downstream AL only while in the firing state. ORNs in the desensitized state had to return to the silent state before firing again. Transitions between states were executed based on random number draws, the number of ORNs in a particular state, and transition propensity parameters (see METHODS and Gillespie 1976). The ORNs in the firing state produced an input current to the AL network, which contained 300 PNs and 100 LNs (see METHODS and Fig. 2*A*). Our stochastic model generated ORN responses similar to those observed in vivo (compare Fig. 2, *B* and *C*, and Fig. 1; see also Raman et al. 2010). By adjusting the parameters governing transition to and recovery from desensitization, we created ORN activity with various levels of adaptation (see Fig. 2*C* and METHODS). Specifically, we found parameters that created P_{adp} values between 0.1 and 0.7 (see METHODS and Table 1) and matched temporal and spatial profiles of ORN in vivo response. ORN input to the AL elicited complex PN responses (see Fig. 2, *D* and *E*) with characteristic LFP oscillations at ~20 Hz (Fig. 2, *F* and *G*; Bazhenov et al. 2001a; Laurent et al. 1996). The computational model of the AL neurons (both PNs and LNs) is based on previous modeling work (Assisi et al. 2007, 2011; Bazhenov et al. 2001a, 2001b, Kee et al. 2015; Sanda et al. 2016). In contrast to our AL model, our new ORN model was constructed to be more computationally efficient, to simulate a large number of ORNs, and to highlight the role of adaptation in olfactory stimulation.

In constructing the ORN model, it was crucial that the model could generate the appropriate concentration dependence, especially considering that we intend to effectively double the concentration when presenting two similar odors simultaneously. However, to the best of our knowledge, there is no systematic study of ORN activity while varying odorant concentration in locusts. Conflicting results have been obtained from different organisms. In the fruit fly (Hallem and Carlson 2006; Kreher et al. 2008), single ORNs can increase firing rates over two orders of magnitude depending on the concentration. In the moth (Ito et al. 2009), the proportion of responsive ORNs increases but maximal firing rate of ORNs does not. We found that our model can reproduce both behaviors depending

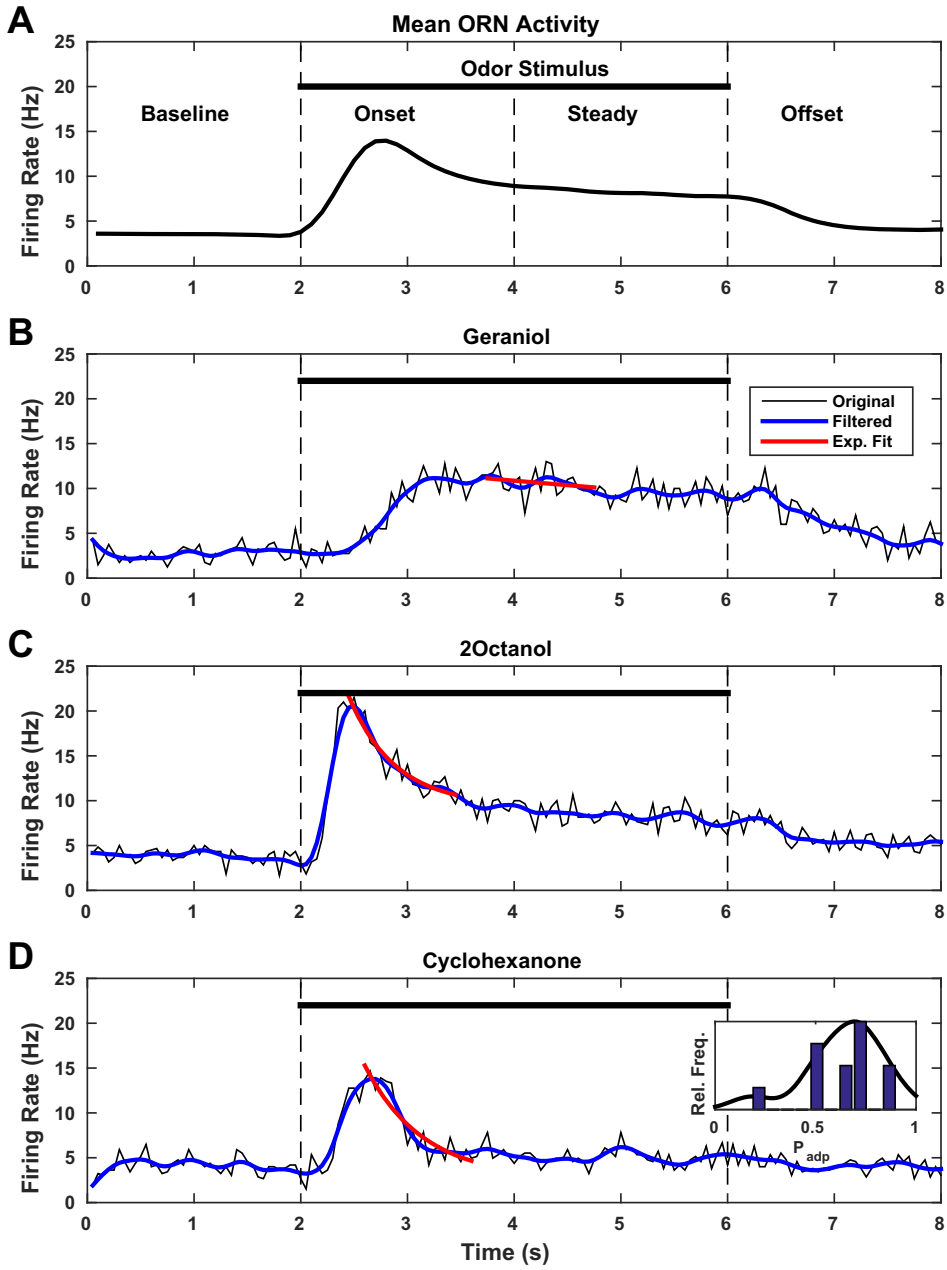

Fig. 1. Variability of olfactory receptor neuron (ORN) adaptation. *A*: mean ORN activity (averaged over 238 ORN-odor pairs) shows 4 distinct phases: baseline, onset, steady, and offset. *B–D*: mean ORN firing rate of different odorants show different kinetics and adaptation rates (geraniol: 16 ORNs, 2-octanol: 24 ORNs, cyclohexanone: 21 ORNs). Shown are raw traces (black), zero-phase filtered (blue), and exponential fit from peak of filtered trace to 1 s forward (red). All odors are presented at the same 1% (vol/vol) dilutions. *Inset* in *D*: histogram, bars, and kernel density estimate (solid black curve) of the distribution of adaptation levels. The kernel density estimate is computed with MATLAB's ksdensity.

on the concentration of the stimulus. At high concentration, ORNs largely responded only by increasing the proportion of responding ORNs and not by increasing peak activity of single ORNs. However, at lower concentration peak ORN activity also increased. The odor concentrations we used for the experiments are phenomenologically closer to what we see in moths (Ito et al. 2009); however, the main findings of our work are not dependent on this.

Adaptation Improved Classification of Dissimilar Odorants

The natural olfactory environment involves complex combinations of many odorants presented simultaneously, which increases the difficulty of odor identification. To quantify the role of ORN adaptation in the response to complex stimuli, we employed in the model a stimulation paradigm similar to that we have used before in vivo (Saha et al. 2013, 2015). The first odor (background odor) was presented for a longer time (8 s). Starting 2 s after the onset of the background odor, during the steady-state phase of background odor adaptation (see Fig. 1), we presented a second odor (foreground odor) for a shorter time (4 s) (Fig. 3*A*). Our model produced ORN population dynamics qualitatively similar to those seen in vivo (Fig. 3*A*, *inset*). Specific discrepancies between the model and experimental responses are largely due to variation of peak ORN response from foreground to background odors. Populations of ORNs in vivo show response variation in multiple different domains including adaptation, peak response, odor similarity, and others. We first set out to study the effects of adaptation alone and therefore restricted ourselves to modeling responses with identical peak response and dissimilar background and foreground odors. We defined dissimilar odors as those that have little to no overlap in the inputs to ORNs (see Fig. 3*A*,

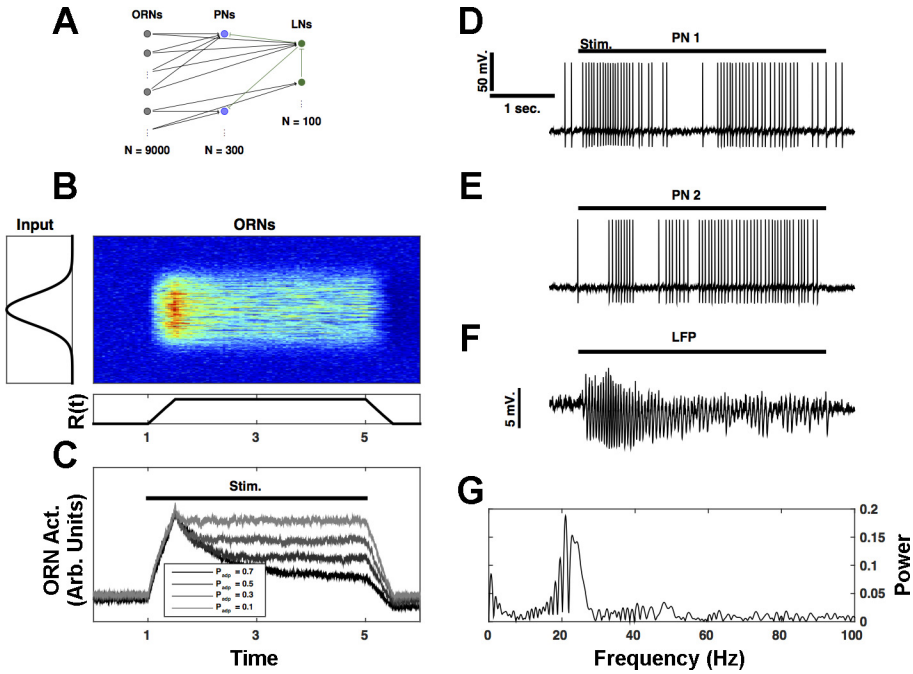

Fig. 2. Model of the first 2 stages of olfactory pathway. *A*: the model olfactory circuit consists of 9,000 olfactory receptor neurons (ORNs) that project to 300 projection neurons (PNs) and 100 local neurons (LNs) in the antennal lobe. The LNs make GABAergic synapses (green) on PNs and other LNs. The PNs make AMPA synapses (black arrows) onto LNs and project to downstream neural structures. *B*: activity of model ORNs with spatial (*y*-axis) and temporal (*x*-axis) dependence. Because of the large number of ORNs, we show the average of 30 ORNs on the spatial scale. Hotter colors indicate stronger activity. The color range denotes 0–11 Hz. Spatial dependence of input intensity to the ORN model (*left*) is Gaussian, and temporal dependence of input intensity, $R(t)$, is given by a linear ramp up and down in time (*bottom*). See METHODS for details. *C*: ORN activity summed over all ORNs for various levels of ORN adaptation (P_{adp}). *D* and *E*: odor-evoked spiking responses of sample PNs. *F*: local field potential (LFP) computed as the average of model PN voltage. *G*: power spectrum of the sample LFP shown in *F* calculated with standard fast Fourier transform methods.

left). We then asked whether the neural representation of the foreground odor was disrupted by the presence of the background odor. We have previously explored in vivo the role of time delays between foreground and background presentations (Saha et al. 2013) and found that even small delays between background and foreground odor onsets are sufficient to correctly recognize foreground odorants. Here we focus on adaptation and odor similarity.

To quantify the success of odor recognition by AL neurons, we used a classification algorithm we developed previously (Saha et al. 2013, 2015). First, we summed PN firing activity in 50-ms nonoverlapping time bins and created a high-dimensional representation of PN responses to odorants, where each spatial dimension is given by the number of spikes of each specific PN and the temporal dimension is given by the specific bin number. At each time bin, we compared the high-dimen-

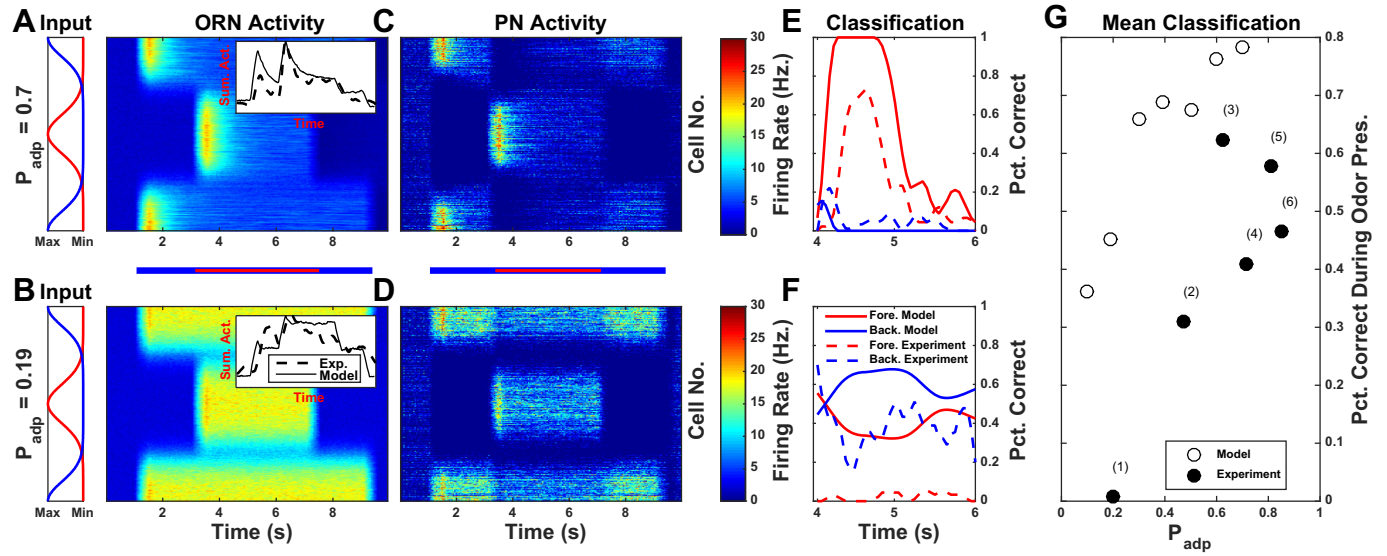

Fig. 3. Adaptation increases classification of foreground odor in presence of a dissimilar background. *A* and *B*: simulation of olfactory receptor neuron (ORN) activity for highly adapting odors and less adapting odors. Activity is averaged over 30 ORNs [denoting the input to single projection neurons (PNs)] and binned in 50-ms bins. Hotter colors indicate higher ORN responses; units are arbitrary. Blue and red bars denote timing of background and foreground stimulus, respectively. *Left*: spatial profile of input for background (blue) and foreground (red) odors. P_{adp}, level of ORN adaptation. *Inset*: comparison to experimental results. *C* and *D*: mean PN activity for highly adapting (*C*) and less adapting (*D*) odors, binned in 50-ms bins. Note that PN responses in *C* and *D* are simulated from the ORN inputs obtained from *A* and *B*, respectively. *E* and *F*: classification of the overlap (foreground on top of background) as solitary foreground or background odor is compared between the model and experimental results averaged over 10 trials. Color indicates the odor template identified in the classification algorithm (red, foreground; blue, background, also see METHODS). Comparison of model vs. experiment is shown in each case. Classification begins at onset of foreground odor. To obtain smoother curves, classification rates are put through a 3-point moving average filter. *G*: mean classification over peak of foreground odor presentation (first 0.75 s) for various levels of adaptation. Odor pairs: *1*, geraniol (Back.)–citral (Fore.); *2*, mint (Back.)–apple (Fore.); *3*, hexanal (Back.)–hexanol (Fore.); *4*, 2-octanol (Back.)–hexanol (Fore.); *5*, benzaldehyde (Back.)–isoamyl acetate (Fore.); *6*, cyclohexanone (Back.)–2-heptanone (Fore.).

sional response vector of the overlap of the foreground and background odors (hereafter called simply overlap) to the high-dimensional response of the foreground odor alone and to background odor alone by determining the minimal angular distance in the high-dimensional space. It should be noted that our algorithm requires certain criteria to be met in order to classify an odor. Hence, not all points will be classified as either foreground or background (see METHODS).

Averaging over 10 trials, we obtained classification functions giving time-dependent pattern-matching results of overlap to foreground and overlap to background odors (Fig. 3, *E* and *F*, respectively). The classification success of model results largely depended on the sources of variance between different trials of the same odorant, which were driven by the stochastic nature of the ORN model (see METHODS). The results from model simulations were compared to those of in vivo recordings. Odorants that had strong adaptation showed high classification success ($P_{adp} = 0.7$ is shown in Fig. 3, *A*, *C*, and *E*). When we performed the same experiment with odors that adapt less ($P_{adp} = 0.19$ is shown in Fig. 3, *B*, *D*, and *F*), the classification success of foreground was significantly reduced. In general, we report that mean classification success when compared between dissimilar background and foreground odor pairs, both in model simulations and in vivo, depends strongly on the level of adaptation of the ORNs, P_{adp} (Fig. 3*G*). Higher values of classification are seen in the model because other considerations, such as odor similarity, have not yet been accounted for.

Adaptation Primed AL Circuit for Novelty Detection

Adaptation of the ORNs offers an advantage in recognizing multiple odors in a complex environment. Increasing ORN adaptation diminishes the impact of the background odorants on the downstream AL circuit and enhances impact of the foreground odors. But how would this change the spatiotemporal pattern of population PN responses?

To investigate the mechanism by which adaptation increases classification success in the AL during complex odor presentations, we employ dimensionality reduction techniques to visualize the effect of adaptation on model PN responses. High-dimensional responses were projected onto the first three principal directions (eigenvectors of the response covariance matrix corresponding to largest eigenvalues) that accounted for maximum variance in the data by principal component analysis (PCA). These directions were determined on the basis of the variance of PN firing rate over time and stochastic trials during all three conditions (foreground, background, and overlap) jointly. Our modeling results were qualitatively similar to those found with in vivo recordings (Mazor and Laurent 2005; Raman et al. 2010; Saha et al. 2015). Solitary foreground and background trajectories originated from baseline levels, underwent a large transient, and then remained near the fixed point until odor offset, when they returned to baseline (Fig. 4*A*). Overlap trajectories, as the presentation of the foreground odor on top of the background odor, originated from the background fixed point and projected toward the foreground trajectory (Fig.

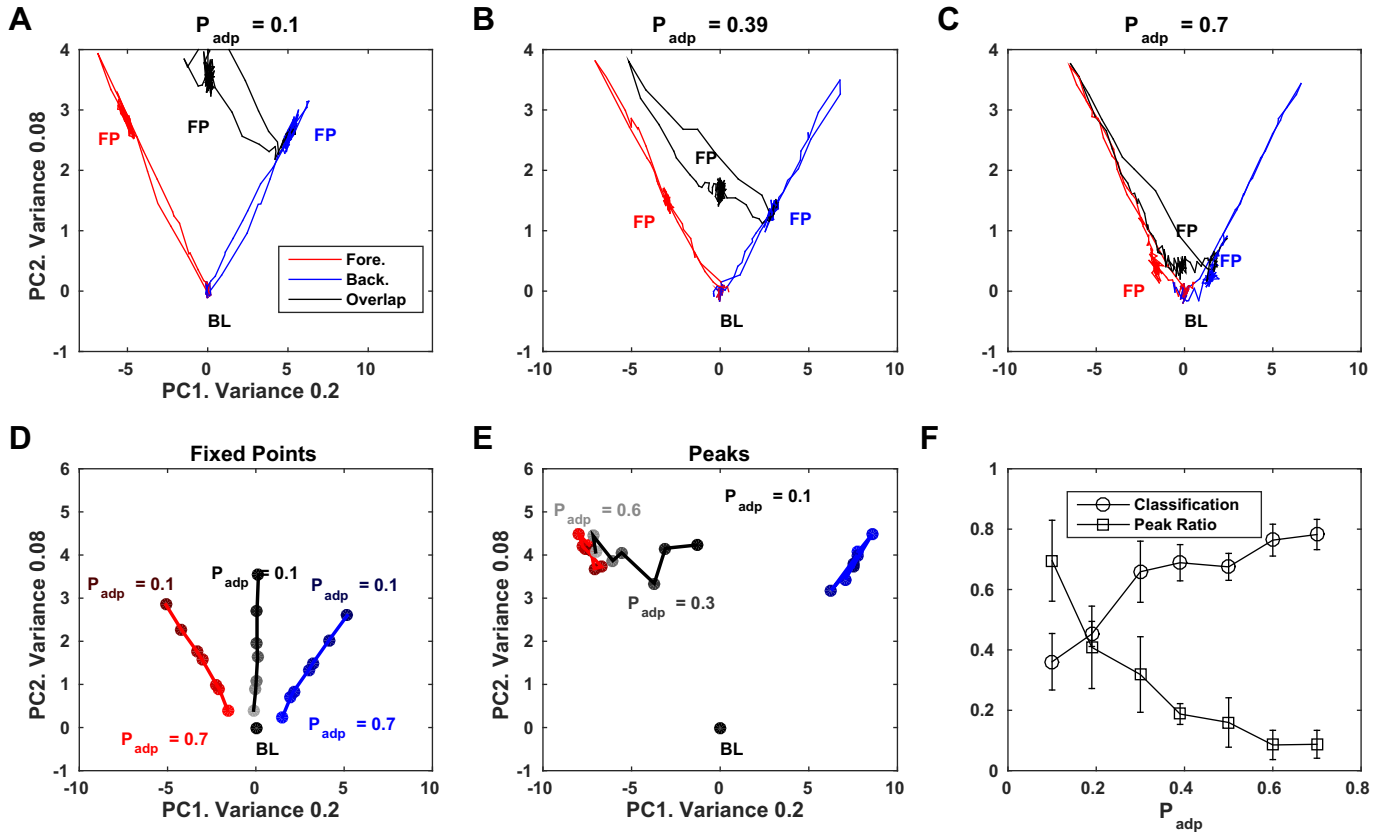

Fig. 4. Adaptation resets the model antennal lobe. *A–C*: odor trajectories in principal component analysis (PCA) space for foreground, background, and overlap presentations at various levels of adaptation (P_{adp}). Fixed point (FP) and baseline (BL) are identified in each trajectory. *D*: FPs from all adaptation levels are plotted on a single axis. Brighter colors refer to more adaptation. *E*: trajectory peaks are plotted for all adaptation levels on a single axis. *F*: classification probability and peak ratio (overlap vs. foreground from PCA) are plotted for different adaptation levels. Error bars represent SD over trials.

4, *A–C*). We found that increasing adaptation of ORNs changed the location of the stationary fixed points, bringing fixed points of the each stimulus type (solitary foreground, solitary background, and overlap) closer to the baseline stationary point (Fig. 4*D*). Thus increasing ORN adaptation brought the origin of the overlap trajectory closer to the baseline stationary point and therefore aligned the overlap trajectory better with the foreground trajectory. We quantified this alignment by calculating the distance between the peak (maximal norm of PCA trajectory) of the foreground and overlap trajectories (Fig. 4*E*). We found that the alignment of foreground and overlap peaks correlated with higher classification (Fig. 4*F*). We qualify this action of adaptation (bringing the steady state or "fixed point" closer to the baseline) as "priming for novelty," since it brings the system close to its prestimulus state.

The main contribution of receptor adaptation in resolving distinct odors is the attenuation of the competing background odor signal. Adaptation desensitizes ORNs to constant background stimuli, and this resets the olfactory system to be sensitive to novel, and distinct, odorants. We showed that the odor-evoked trajectory of PNs, which are one synapse downstream of ORNs, is transformed by ORN adaptation. Specifically, activity in the AL after adaptation was "close," in PCA space, to the baseline: priming for novelty. In contrast, odorants that did not adapt showed distinctive PCA trajectories, between solitary and overlap presentations, and poor classification. However, we have restricted the scope of the complex environment to concurrent presentations of "dissimilar" odorants.

Similar Odors Caused Interference Leading to Poor Odor Recognition

To investigate the effect of ORN adaptation on representations of the foreground odorants in the presence of similar background odorants, we created inputs to our model ORNs with various degree of overlap (Fig. 5, *A* and *B*, *left insets*). We found that similar odors can cause selective interference in an adaptation-specific manner. Specifically, in response to the foreground odor in the presence of a similar background odor that adapted significantly, spikes were lost from the population of PNs that are coactivated by both odorants (Fig. 5*D*, *PNs*

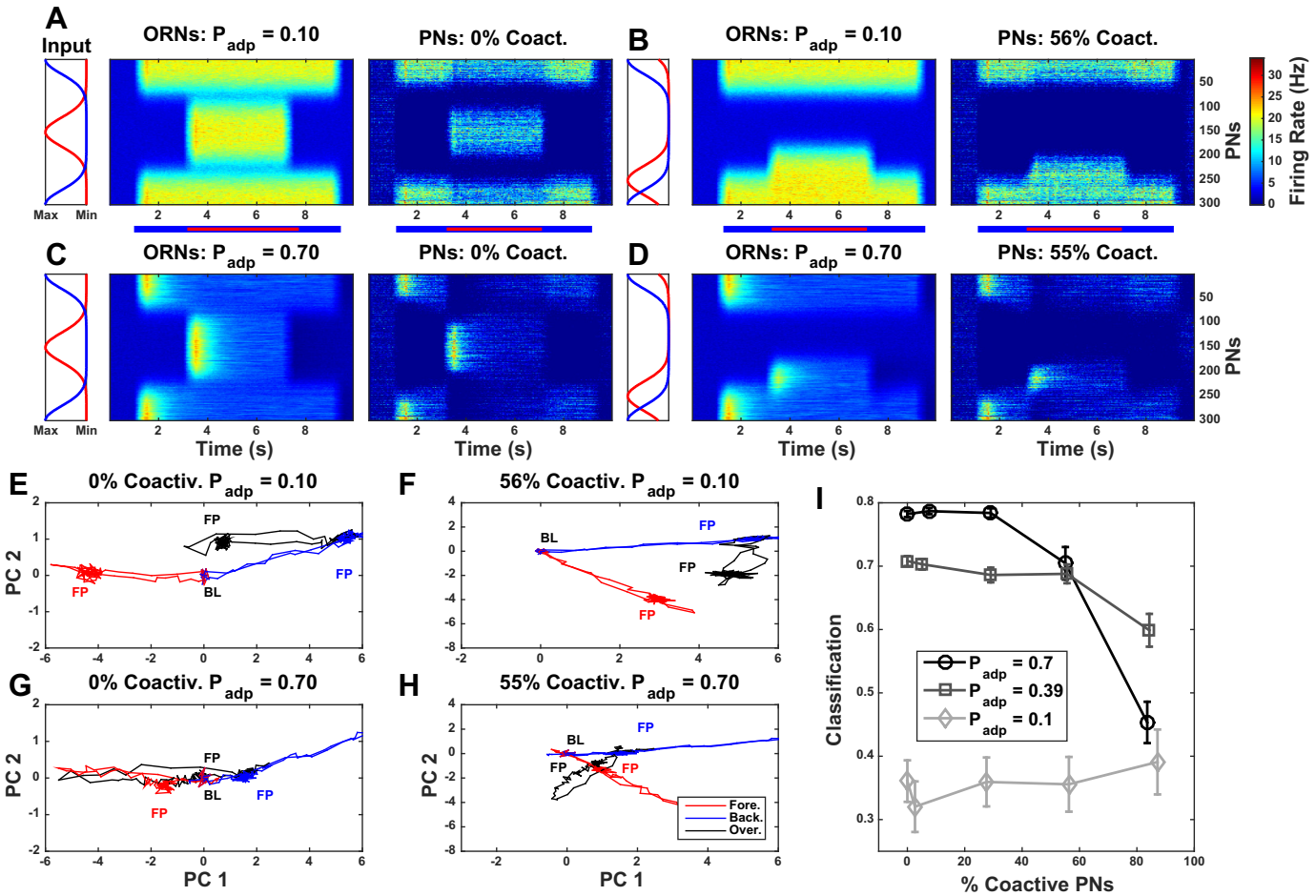

Fig. 5. Olfactory receptor neuron (ORN) adaptation has a differential impact on odor recognition depending on the similarity between the odors. *A*: input to ORNs (*left*), mean ORN activity (*center*), and projection neuron (PN) activity (*right*) for dissimilar odorants (0% coactivation) with little adaptation [level of ORN adaptation (P_{adp}) = 0.1]. Consistent with previous work (Saha et al. 2015), we quantified the similarity of odors by % of PNs that were activated in solitary presentations of both odorants ("coactivated," see METHODS). Hotter colors indicate higher ORN responses; units are arbitrary. *B–D*: similar plots are given for odorants with varying similarity and adaptation. *E–H*: corresponding principal component analysis (PCA) trajectories of foreground (red), background (blue), and overlap (black) conditions for the odors shown in *A–D*, respectively. Fixed point (FP) and baseline (BL) are identified in each trajectory. *I*: variations in foreground classification as the similarity between foreground and background odor changes. Different symbols correspond to different adaptation levels (P_{adp}). Error bars denote SE over trials.

250–300). At the same time, similar odors that did not adapt showed little to no loss of PN spikes (compare Fig. 5, *B* vs. *D*, *PNs 250–300*). We showed in *Adaptation Primed AL Circuit for Novelty Detection* that increases in adaptation increased alignment of the PCA trajectories between foreground and overlap conditions for dissimilar odors (compare Fig. 5, *E* vs. *G*). In contrast, analysis of the PCA trajectories of the similar odors revealed that the overlap trajectory for similar odorants with large adaptation overshot the foreground target trajectory, indicating a response misalignment (compare Fig. 5, *G* vs. *H*) adaptation. This misalignment was mirrored by a decrease in classification rate with increased coactivation in the case of strongly adapting background odor. Classification dropped as similarity increased when adaptation was moderate as well. When adaptation was minimal, classification was largely independent of similarity (Fig. 5*I*).

Thus adaptation has differential effects on classification depending on the similarity between odorants. When odors are dissimilar, ORN adaptation resets the olfactory system after long presentations of background odors to allow for robust representations of foreground odors. However, when odors are similar, our model predicts that ORN adaptation causes the specific loss of spikes from PNs that are coactivated by both foreground and background odors. This spike loss only occurs when odors are similar and adaptation is high.

Loss of Spikes from Coactivated PNs in Model and in Vivo

Our model predicts that neural representation of similar odorants can be altered when a foreground odor is presented on top of a highly adapting background odor. This mechanism should lead to specific observations in experimental data. We predict that the peak of PN responses would decrease during the overlap (foreground in the presence of background odors) relative to the solitary (foreground only) presentations. Concurrent stimulation of similar odors leads to a population of already adapted receptor neurons (from stimulation of the background odor) that significantly reduce their response to the foreground odor because of adaptation: the coactivated population. Thus PN activity loss should come specifically from the population of PNs that are coactivated by both foreground and background odors. Furthermore, we predict that reduction in the peak of PN activity would scale with the size of the coactivated population, a measure of odor similarity.

Indeed, we found strong agreement between these model predictions and experimental recordings (Fig. 6) (see also Saha et al. 2015). Both model and experiment showed statistically significant reduction of the peak activity in response to the foreground odor during its presentation on the top of a similar background odor (Fig. 6, *C* and *D*; model: $P = 5.1 \times 10^{-7}$, experiment: $P = 5.3 \times 10^{-4}$). This reduction was not present during simultaneous presentation of the dissimilar odors (compare Fig. 6, *A* and *B*; model: $P = 0.34$, experiment: $P = 0.30$).

To evaluate the cause of this reduction in PN activity, we segregated PNs into three different populations of responsive PNs: PNs responsive to foreground odor only, PNs responsive to background odor only, and coactivated population of PNs (responsive to both). Each PN was deemed responsive to a specific odor if its activity increased significantly above baseline during the presence of that odor (see METHODS). Our model predicts that activity loss during overlapping odor presentations should come from the spikes in the coactivated PN population. Similar odor pairs that had a significant drop in activity revealed that this reduction depended on the coactivated PN population both in the model (Fig. 6*E*) and in experiment (Fig. 6*F*). Our modeling results predict that increasing amounts of spikes will be lost from the coactivated population with increasing odor similarity and adaptation (Fig. 6*G*). In extreme cases, very high adaptation and very similar odors, we found that this coactivated activity decreased even below levels seen during adapted background odor stimulation (2 s after odor stimulation: the portion aligned with overlap stimulus). In other words, exposure to foreground on top of background removed spikes from the neural representation of the background odor. Although the trend is not as clear as in the model, we found that both adaptation and similarity increase the magnitude and significance of the coactivated PN loss in experimental data (Fig. 6*H*). The relationship may not be as clear in the experimental case because of the small number of odor pairs (12) and unaccounted sources of variation (such as variability in the peak ORN response). However, the agreement between model and experiment is very clear when comparing odor similarity alone (Fig. 6*I*).

Adaptation Altered Odor Representation Highlighting Novel Components

The natural environment may include presentations of complex odor mixtures with overlapping components. It is vital for animal survival to reliably detect novel odorants, even in the presence of background odorants. We first investigated the mechanisms of background subtraction, through loss of coactivated activity, in our model. During overlap presentations a higher portion of the coactivated ORN population is in the desensitized state and thus cannot become activated, leading to reduced ORN activity (Fig. 7*A*). This leads to a decrease in input to PNs, as reported earlier. Moreover, we found that coactivated spike loss from PNs was much greater than from ORNs (Fig. 7*B*). This was most likely due to lateral inhibition silencing coactivated PNs with only moderate input. We next sought to determine whether the loss of coactivated PN spikes that we report in this study could lead to an altered odor representation. To investigate this, we created background and foreground odors with both distinct and overlap features (Fig. 7*C*). Here, the background odor is created as a mixture of *components I* and *II*, and the foreground odor is a mixture of *components II* and *III*. These components (*I–III*) may correspond, e.g., to the small chemical compounds with different functional groups like hexanal, hexanol, cyclohexanone. We then tested whether the neural representation was closest to the foreground odor (*II* + *III*), the background odor (*I* + *II*), or a third unique odor formed by the component unique to the foreground odor only and not present in the background odor, *III*. We found that the loss of coactivated PN spikes increased with odor adaptation level, as reported before (Fig. 7, *C–E*), and at the highest levels of adaptation only the unique components of the foreground were identified (Fig. 7, *F–H*). We also found that as the adaptation increased the overlap trajectory aligned more closely with the unique components to the foreground odor (*III*) than either foreground or background trajectories (Fig. 7, *I–K*). Therefore, we conclude that loss of coactivated PN spikes, caused by presentation of a foreground odor on top of

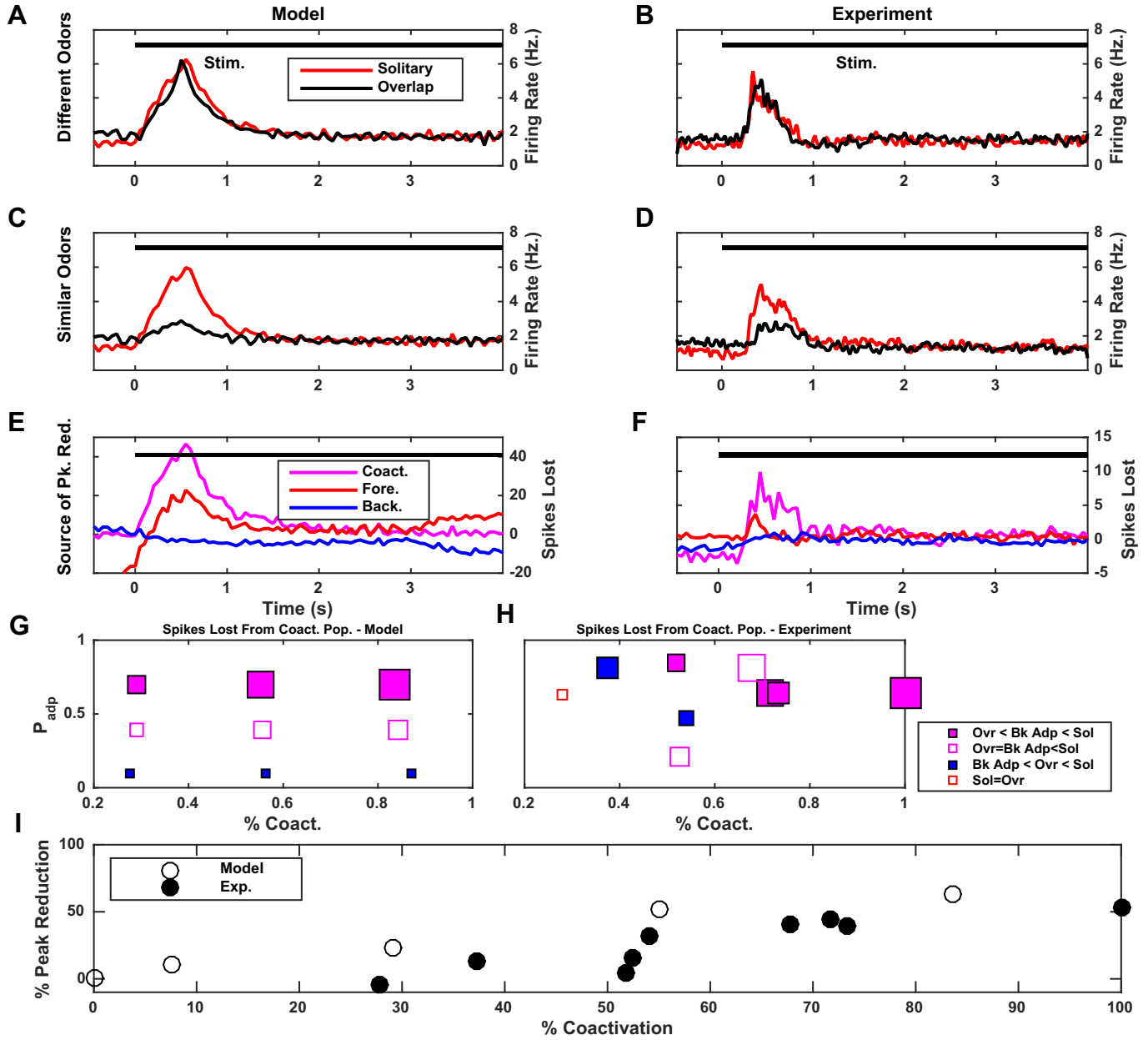

Fig. 6. The peak reduction in projection neuron (PN) activity can be driven by the coactivated olfactory receptor neurons (ORNs). *A*: mean firing rate from the model from all model PNs is shown for an odor pair with low coactivation [level of ORN adaptation (P_{adp}) = 0.7, 0% coactivated PNs] between foreground and background. Both solitary and overlap presentations of the foreground odor are shown. Overlap presentations are aligned to the onset of foreground odor (2 s after background odor). *B*: similar plot as in *A* but now showing the experimental results obtained for dissimilar odor pairs: cyclohexanone (Back.)–2-heptanone (Fore.); n = 116 PNs. *C*: simulation of overlap vs. solitary PN responses are shown for the odors which have higher overlap (P_{adp} = 0.7, 53% coactivated PNs). *D*: similar plot as in *C* but now showing experimental results obtained for a similar odor pair: 2-octanol (Back.)–Hexanol (Fore.); n = 104 PNs. *E*: reduction in firing activity during foreground component of overlap presentation across conditions is compared for different subsets of PNs: coactivated, foreground specific, and background specific. *F*: PN activity loss for different subpopulations is shown for the experimental data. *G*: PN spikes lost from coactivated population over first 2 s of foreground odor stimulation in model simulations. Coloring is based on the presentation with the least amount of spikes. Box size scales linearly to the number of spikes lost in each case. Smallest boxes denote a zero or negative change from solitary to overlap. Largest boxes denote ~1,000 spikes lost in average between the 2 populations. Solid purple boxes denote cases where spikes from overlap presentations were significantly less than both solitary presentations and adapted background presentations (background only 2 s after exposure). Significance was determined by 1-sided t-tests with α = 0.05. Open purple boxes denote scenarios where overlap cases were not significantly different from background adapted levels. Solid blue boxes denote scenario when spikes during overlap presentations were significantly more than background adapted presentations. Red boxes denote scenarios where overlap presentations were not significantly different from solitary presentations. *H*: similar to *G* but using experimental data. Smallest box denotes a loss of ~3 spikes on average; largest box denotes a loss of 100 spikes. Box scaling is different from *H* because of the difference in number of recorded PNs. *I*: coactivation and the peak reduction during overlapping condition is compared between the model (P_{adp} = 0.7) and various odor pairs tested experimentally.

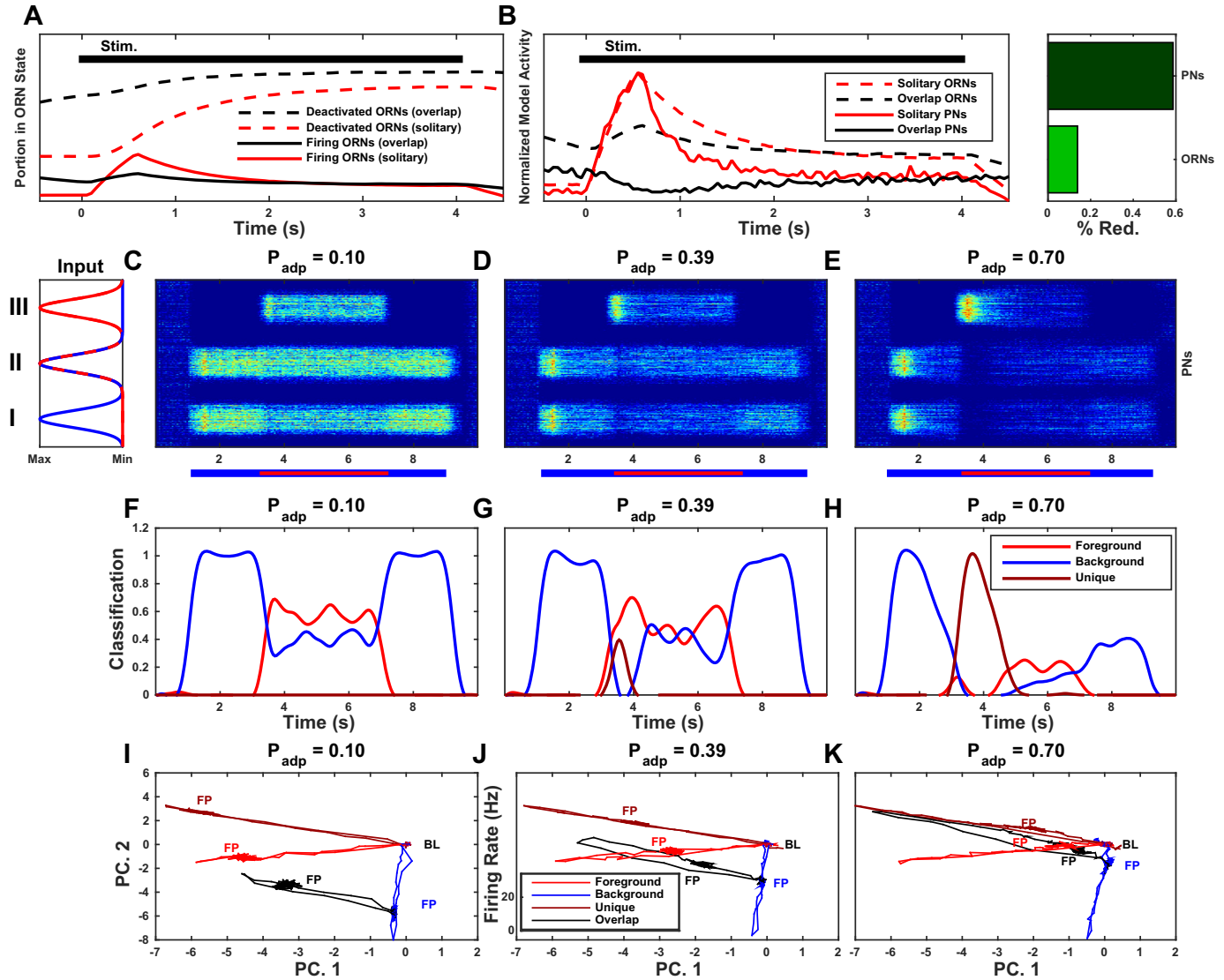

Fig. 7. Similar odorants cause interference. *A*: state of model olfactory receptor neuron (ORN) receptors in the solitary and overlap presentations for highly adapting and similar odors [level of ORN adaptation (P_{adp}) = 0.7, 53% coactivated projection neurons (PNs)]. States are averaged over the coactivated population only. *B*: spike loss from solitary to overlap compared between ORNs and PNs from the coactivated population and quantification (*right*). *C*: input profile to PNs for foreground (red) and background (blue). Dashed area gives the overlap. *C–E*: PN responses at various adaptation levels. *F–H*: classification for corresponding plots as above. *I* and *K*: principal component analysis (PCA) for corresponding plots above. Fixed points (FPs) are given for each trajectory, and a common baseline (BL) level is given for all cases.

the similar background odor, caused an alteration of the foreground representation in favor of unique components.

DISCUSSION

Adaptation is a common feature to many sensory systems. Using a combination of computational modeling and electrophysiology, we found that ORN adaptation can have divergent effects on odor recognition: strong ORN adaptation was beneficial for recognition of the dissimilar foreground odors in the presence of a background odor but altered the representation of foreground odors when background odors were similar.

Diversity of ORN Adaptation

Recordings from the locust antennae (Raman et al. 2010) or individual ORNs (Fig. 1) revealed a characteristic response of the ORNs to olfactory stimulus. Averaged responses of ORNs have previously been regarded as representative of the temporal structure of the output of the antennae. Both computational models (Bazhenov et al. 2001a, 2001b) and electrophysiological recordings (Wehr and Laurent 1999) have shown that the characteristic 20-Hz oscillations recorded in the insect calyx are generated by AL circuitry and occur even when simplistic electrical input is given to the AL. However, dynamic variability characteristics of the PN odor responses, such as outlasting the stimulus and transitioning between periods of excitation and inhibition, require heterogeneous input from the ORNs, such as those elicited by olfactory stimuli (Raman et al. 2010).

Application of specific odorants selects a unique set of responsive ORNs (Hallem and Carlson 2006). Here we report that ORN responses in locusts generate adaptation profiles that ranged between $0.18 < P_{adp} < 0.9$. The specific dynamics, including adaptation, of ORN responses originate with the

individual olfactory receptor kinetics (Hallem et al. 2004). In rodents, individual receptors respond to long odor pulses by accumulating intracellular calcium, which eventually inhibits the receptor and renders it in an inactive state (Ma 2007; Zufall and Leinders-Zufall 2000). In this study we implemented a stochastic state ORN model specifically to incorporate receptor desensitization (Fig. 2 and METHODS). We propose that adaptation of ORNs provides a novel component of the odorant information generated in the antennae by the kinetics of responsive olfactory receptors. This information is then transmitted downstream to the AL, where it is necessary for complex dynamics in the AL.

Adaptation Facilitates Classification of Dissimilar Odors by Priming AL for Novelty Detection

The natural olfactory setting for insects can include pervasive background stimuli. Background odorants can have a variety of impacts on odor-induced behavior of insects (Schröder and Hilker 2008). The identification of ecologically relevant odors (e.g., those indicating food or predators) remains critical. Even in the case of conserved pheromone olfactory pathways, the presence of background odors can alter sensory processing (Renou et al. 2015). Behavioral experiments with locusts revealed a large variance in success in recognizing odorants in a complex background (Saha et al. 2013, 2015). What role does processing at the periphery (i.e., ORN adaptation) have in predicting the success rate of this task?

Our work shows that adaptation has a substantial positive effect on this type of classification when background and foreground odors are dissimilar (Fig. 3). Dimensionality reduction analysis of the PN odor response trajectories revealed that adaptation acts largely by resetting the AL circuitry to prestimulus conditions but leaves the transient activity largely unaffected (Fig. 4). In vivo studies reported that PNs are maximally informative about odor identity in on- and off-transients and less so during steady state (Mazor and Laurent 2005). Adaptation allows the AL to desensitize to persistent background odors without altering the informative component of these odors, the on-transient. Subsequently, by the time when the substantially dissimilar foreground odor is applied, adaptation has nearly reset the AL and representations of the foreground odors occur as though there was no background odor at all.

Adaptive responses to background odors have been shown previously in the extraction of salient information from a complex odor environment in rats (Kadohisa and Wilson 2006; Linster et al. 2007). However, in this case the origin of neural adaptation occurred centrally. Our work demonstrates that in locusts this adaptation can occur at the first neuron in the olfactory system and this adaptation has a direct impact on downstream odor recognition (Fig. 3).

Adaptation Alters Representation of Similar Odors

Discriminating similar odors is a hard task for locusts. When this task is performed in the context of a background odorant, locusts show a highly variable success rate (Saha et al. 2015). Our work demonstrates that adaptation of ORNs interferes with this task, an effect we denote similar odor interference. The interference is a direct consequence of the decrease in firing rate in the PNs that are responsive to both background and foreground odors, the coactivated PNs.

In our model, the loss of coactivated PN spikes can be explained by a two-stage mechanism. In the antenna, during the steady-state phase of the background odor presentation but before the onset of the foreground odor, ORNs in the overlap of both odorants are pushed into the desensitized state (Fig. 7*A*). When the foreground odor is later presented, these ORNs cannot respond to the foreground odor because they have been desensitized. In the AL, PNs downstream of this subset of ORNs will receive muted input, leaving them vulnerable to the lateral inhibition from LNs. Therefore, when odors share ORN populations that respond with highly adapting firing rates, peak activity will be less in the overlap (background over foreground) presentations than in the solitary foreground presentations (Fig. 7*B*). This effect should vary with the degree of similarity as seen in vivo (Saha et al. 2015).

Our model predicted that the variance in success of identifying foreground odors over background, as reported in vivo (Saha et al. 2013, 2015), may be due to interference of similar background and foreground odor representations. Indeed, our experimental results revealed that *1*) peak activity of AL drops during overlap presentations of similar odors, *2*) this drop comes primarily from the coactivated population, and *3*) the magnitude of this drop is predicted by the odor similarity and thus the size of the coactivated population. Our modeling results further predict that adaptation of ORNs during the presentation of similar background odors selects only for novel components of similar odorants (Fig. 7). This phenomenon is similar to nonassociative learning in honeybees, where frequent applications of an unrewarded background odor shifted the representation of odor mixtures toward the novel component (Chen et al. 2015; Locatelli et al. 2013). These results, and our own, suggest that novelty detection is a critical component in insect olfaction across multiple species.

We have previously discussed the relationship between odor similarity and loss of synchrony, which was quantified by the peak activity drop during overlap odor presentations (Saha et al. 2015). We proposed that loss in peak activity from overlap to solitary presentations was in part due to interference in the temporal component of the odor coding (such as jittering of PN spikes). Here we report that another factor accounting for this peak activity loss is deletion of spikes from the coactivated population of PNs during the first second of stimulus.

We found in computational models and experiments that similar odor interference alters the neural representation of the foreground odor. But might this interference go so far as to trick the animal into believing that a completely different odorant was presented? Our modeling results show that similar odor interference realigns foreground representations, demonstrating a type of hysteresis in the olfactory representation scheme. Whether this may lead to misclassification of olfactory behavior remains to be shown.

Conclusions

Adaptation of the primary sensory neurons plays a critical role in resetting neural systems to allow for novel stimuli. We showed that this strategy could be also employed in the insect olfactory system. However, adaptation leads to surprisingly different effects on the robustness of odor representation de-

pending on ORN adaptation level and odor similarity. Our results provide a novel insight into the strengths and vulnerabilities of a ubiquitous coding strategy, adaptation, in the specific case of insect olfaction.

GRANTS

This work is supported by grants from the National Heart, Lung, and Blood Institute (T32HL134632) awarded to S. Haney, the Office of Naval Research grant (N00014-16-1-2426) awarded to D. Saha, the National Institute on Deafness and Other Communications Disorders (Collaborative Research in Computational Neuroscience: 1 ROB DC-012943) awarded to M. Bazhenov, and the National Science Foundation (IIS-1724405) awarded to M. Bazhenov.

DISCLOSURES

No conflicts of interest, financial or otherwise, are declared by the authors.

ENDNOTE

At the request of the authors, readers are herein alerted to the fact that additional materials related to this manuscript may be found at the institutional Web site of the authors, which at the time of publication they indicate is: https://www.bazhlab.ucsd.edu/downloads/. These materials are not a part of this manuscript and have not undergone peer review by the American Physiological Society (APS). APS and the journal editors take no responsibility for these materials, for the Web site address, or for any links to or from it.

AUTHOR CONTRIBUTIONS

S.H., D.S., B.R., and M.B. conceived and designed research; S.H. and D.S. performed experiments; S.H. and D.S. analyzed data; S.H., D.S., B.R., and M.B. interpreted results of experiments; S.H. prepared figures; S.H. drafted manuscript; S.H., D.S., B.R., and M.B. edited and revised manuscript; S.H., D.S., B.R., and M.B. approved final version of manuscript.

REFERENCES

Assisi C, Stopfer M, Bazhenov M. Using the structure of inhibitory networks to unravel mechanisms of spatiotemporal patterning. *Neuron* 69: 373–386, 2011. doi:10.1016/j.neuron.2010.12.019.

Assisi C, Stopfer M, Bazhenov M. Excitatory local interneurons enhance tuning of sensory information. *PLOS Comput Biol* 8: e1002563, 2012. doi:10.1371/journal.pcbi.1002563.

Assisi C, Stopfer M, Laurent G, Bazhenov M. Adaptive regulation of sparseness by feedforward inhibition. *Nat Neurosci* 10: 1176–1184, 2007. doi:10.1038/nn1947.

Bazhenov M, Stopfer M, Rabinovich M, Abarbanel HD, Sejnowski TJ, Laurent G. Model of cellular and network mechanisms for odor-evoked temporal patterning in the locust antennal lobe. *Neuron* 30: 569–581, 2001a. doi:10.1016/S0896-6273(01)00286-0.

Bazhenov M, Stopfer M, Rabinovich M, Huerta R, Abarbanel HD, Sejnowski TJ, Laurent G. Model of transient oscillatory synchronization in the locust antennal lobe. *Neuron* 30: 553–567, 2001b. doi:10.1016/S0896-6273(01)00284-7.

Brown SL, Joseph J, Stopfer M. Encoding a temporally structured stimulus with a temporally structured neural representation. *Nat Neurosci* 8: 1568–1576, 2005. doi:10.1038/nn1559.

Burns ME, Baylor DA. Activation, deactivation, and adaptation in vertebrate photoreceptor cells. *Annu Rev Neurosci* 24: 779–805, 2001. doi:10.1146/annurev.neuro.24.1.779.

Chen JY, Marachlian E, Assisi C, Huerta R, Smith BH, Locatelli F, Bazhenov M. Learning modifies odor mixture processing to improve detection of relevant components. *J Neurosci* 35: 179–197, 2015. doi:10.1523/JNEUROSCI.2345-14.2015.

Dalton P. Psychophysical and behavioral characteristics of olfactory adaptation. *Chem Senses* 25: 487–492, 2000. doi:10.1093/chemse/25.4.487.

Destexhe A, Mainen ZF, Sejnowski TJ. Synthesis of models for excitable membranes, synaptic transmission and neuromodulation using a common kinetic formalism. *J Comput Neurosci* 1: 195–230, 1994. doi:10.1007/BF00961734.

Galizia CG, Sachse S. Odor coding in insects. In: *The Neurobiology of Olfaction* (Frontiers in Neuroscience), edited by Menini A. Boca Raton, FL: CRC/Taylor & Francis, 2010.

Gillespie DT. A general method for numerically simulating the stochastic time evolution of coupled chemical reactions. *J Comput Phys* 22: 403–434, 1976. doi:10.1016/0021-9991(76)90041-3.

Gillespie DT. Exact stochastic simulation of coupled chemical reactions. *J Phys Chem* 81: 2340–2361, 1977. doi:10.1021/j100540a008.

Hallem EA, Carlson JR. Coding of odors by a receptor repertoire. *Cell* 125: 143–160, 2006. doi:10.1016/j.cell.2006.01.050.

Hallem EA, Ho MG, Carlson JR. The molecular basis of odor coding in the *Drosophila* antenna. *Cell* 117: 965–979, 2004. doi:10.1016/j.cell.2004.05.012.

Hardie RC, Raghu P. Visual transduction in *Drosophila*. *Nature* 413: 186–193, 2001. doi:10.1038/35093002.

Hendin O, Horn D, Hopfield JJ. Decomposition of a mixture of signals in a model of the olfactory bulb. *Proc Natl Acad Sci USA* 91: 5942–5946, 1994. doi:10.1073/pnas.91.13.5942.

Hodgkin AL, Huxley AF. A quantitative description of membrane current and its application to conduction and excitation in nerve. *J Physiol* 117: 500–544, 1952. doi:10.1113/jphysiol.1952.sp004764.

Hudspeth AJ, Gillespie PG. Pulling springs to tune transduction: adaptation by hair cells. *Neuron* 12: 1–9, 1994. doi:10.1016/0896-6273(94)90147-3.

Huguenard JR, Coulter DA, Prince DA. A fast transient potassium current in thalamic relay neurons: kinetics of activation and inactivation. *J Neurophysiol* 66: 1304–1315, 1991. doi:10.1152/jn.1991.66.4.1304.

Ito I, Bazhenov M, Ong RC, Raman B, Stopfer M. Frequency transitions in odor-evoked neural oscillations. *Neuron* 64: 692–706, 2009. doi:10.1016/j.neuron.2009.10.004.

Kadohisa M, Wilson DA. Olfactory cortical adaptation facilitates detection of odors against background. *J Neurophysiol* 95: 1888–1896, 2006. doi:10.1152/jn.00812.2005.

Kee T, Sanda P, Gupta N, Stopfer M, Bazhenov M. Feed-forward versus feedback inhibition in a basic olfactory circuit. *PLOS Comput Biol* 11: e1004531, 2015. doi:10.1371/journal.pcbi.1004531.

Korn G, Korn T. *Handbook of Mathematics*. Moscow: GFML, 1968.

Kreher SA, Mathew D, Kim J, Carlson JR. Translation of sensory input into behavioral output via an olfactory system. *Neuron* 59: 110–124, 2008. doi:10.1016/j.neuron.2008.06.010.

Laurent G. Dynamical representation of odors by oscillating and evolving neural assemblies. *Trends Neurosci* 19: 489–496, 1996. doi:10.1016/S0166-2236(96)10054-0.

Laurent G, Davidowitz H. Encoding of olfactory information with oscillating neural assemblies. *Science* 265: 1872–1875, 1994. doi:10.1126/science.265.5180.1872.

Laurent G, Seymour-Laurent KJ, Johnson K. Dendritic excitability and a voltage-gated calcium current in locust nonspiking local interneurons. *J Neurophysiol* 69: 1484–1498, 1993. doi:10.1152/jn.1993.69.5.1484.

Laurent G, Wehr M, Davidowitz H. Temporal representations of odors in an olfactory network. *J Neurosci* 16: 3837–3847, 1996. doi:10.1523/JNEUROSCI.16-12-03837.1996.

Leitch B, Laurent G. GABAergic synapses in the antennal lobe and mushroom body of the locust olfactory system. *J Comp Neurol* 372: 487–514, 1996. doi:10.1002/(SICI)1096-9861(19960902)372:4<487::AID-CNE1>3.0.CO;2-0.

Linster C, Henry L, Kadohisa M, Wilson DA. Synaptic adaptation and odor-background segmentation. *Neurobiol Learn Mem* 87: 352–360, 2007. doi:10.1016/j.nlm.2006.09.011.

Locatelli FF, Fernandez PC, Villareal F, Muezzinoglu K, Huerta R, Galizia CG, Smith BH. Nonassociative plasticity alters competitive interactions among mixture components in early olfactory processing. *Eur J Neurosci* 37: 63–79, 2013. doi:10.1111/ejn.12021.

Ma M. Encoding olfactory signals via multiple chemosensory systems. *Crit Rev Biochem Mol Biol* 42: 463–480, 2007. doi:10.1080/10409230701693359.

Mazor O, Laurent G. Transient dynamics versus fixed points in odor representations by locust antennal lobe projection neurons. *Neuron* 48: 661–673, 2005. doi:10.1016/j.neuron.2005.09.032.

Perez-Orive J, Mazor O, Turner GC, Cassenaer S, Wilson RI, Laurent G. Oscillations and sparsening of odor representations in the mushroom body. *Science* 297: 359–365, 2002. doi:10.1126/science.1070502.

Pouzat C, Mazor O, Laurent G. Using noise signature to optimize spike-sorting and to assess neuronal classification quality. *J Neurosci Methods* 122: 43–57, 2002. doi:10.1016/S0165-0270(02)00276-5.

Raman B, Joseph J, Tang J, Stopfer M. Temporally diverse firing patterns in olfactory receptor neurons underlie spatiotemporal neural codes for odors. *J Neurosci* 30: 1994–2006, 2010. doi:10.1523/JNEUROSCI.5639-09.2010.

Renou M, Party V, Rouyar A, Anton S. Olfactory signal coding in an odor background. *Biosystems* 136: 35–45, 2015. doi:10.1016/j.biosystems.2015.06.001.

Ricci AJ, Wu YC, Fettiplace R. The endogenous calcium buffer and the time course of transducer adaptation in auditory hair cells. *J Neurosci* 18: 8261–8277, 1998. doi:10.1523/JNEUROSCI.18-20-08261.1998.

Riffell JA, Lei H, Hildebrand JG. Neural correlates of behavior in the moth *Manduca sexta* in response to complex odors. *Proc Natl Acad Sci USA* 106: 19219–19226, 2009. doi:10.1073/pnas.0910592106.

Rokni D, Hemmelder V, Kapoor V, Murthy VN. An olfactory cocktail party: figure-ground segregation of odorants in rodents. *Nat Neurosci* 17: 1225–1232, 2014. doi:10.1038/nn.3775.

Saha D, Leong K, Li C, Peterson S, Siegel G, Raman B. A spatiotemporal coding mechanism for background-invariant odor recognition. *Nat Neurosci* 16: 1830–1839, 2013. doi:10.1038/nn.3570.

Saha D, Li C, Peterson S, Padovano W, Katta N, Raman B. Behavioural correlates of combinatorial versus temporal features of odour codes. *Nat Commun* 6: 6953, 2015. doi:10.1038/ncomms7953.

Sanda P, Kee T, Gupta N, Stopfer M, Bazhenov M. Classification of odorants across layers in locust olfactory pathway. *J Neurophysiol* 115: 2303–2316, 2016. doi:10.1152/jn.00921.2015.

Schröder R, Hilker M. The relevance of background odor in resource location by insects: a behavioral approach. *BioScience* 58: 308–316, 2008. doi:10.1641/B580406.

Simões P, Ott SR, Niven JE. Associative olfactory learning in the desert locust, *Schistocerca gregaria*. *J Exp Biol* 214: 2495–2503, 2011. doi:10.1242/jeb.055806.

Sloper JJ, Powell TP. Ultrastructural features of the sensori-motor cortex of the primate. *Philos Trans R Soc Lond B Biol Sci* 285: 124–139, 1979. doi:10.1098/rstb.1979.0002.

Stopfer M, Bhagavan S, Smith BH, Laurent G. Impaired odour discrimination on desynchronization of odour-encoding neural assemblies. *Nature* 390: 70–74, 1997. doi:10.1038/36335.

Stopfer M, Jayaraman V, Laurent G. Intensity versus identity coding in an olfactory system. *Neuron* 39: 991–1004, 2003. doi:10.1016/j.neuron.2003.08.011.

Traub RD, Jefferys JG, Whittington MA. Simulation of gamma rhythms in networks of interneurons and pyramidal cells. *J Comput Neurosci* 4: 141–150, 1997. doi:10.1023/A:1008839312043.

Verhagen JV, Wesson DW, Netoff TI, White JA, Wachowiak M. Sniffing controls an adaptive filter of sensory input to the olfactory bulb. *Nat Neurosci* 10: 631–639, 2007. doi:10.1038/nn1892.

Wehr M, Laurent G. Odour encoding by temporal sequences of firing in oscillating neural assemblies. *Nature* 384: 162–166, 1996. doi:10.1038/384162a0.

Wehr M, Laurent G. Relationship between afferent and central temporal patterns in the locust olfactory system. *J Neurosci* 19: 381–390, 1999. doi:10.1523/JNEUROSCI.19-01-00381.1999.

Zufall F, Leinders-Zufall T. The cellular and molecular basis of odor adaptation. *Chem Senses* 25: 473–481, 2000. doi:10.1093/chemse/25.4.473.